



CrossMark  
click for updates

Cite this: *RSC Adv.*, 2016, 6, 92648

# Aldehyde-functionalized porous nanocellulose for effective removal of heavy metal ions from aqueous solutions

C. Yao,<sup>a</sup> F. Wang,<sup>a</sup> Z. Cai<sup>\*b</sup> and X. Wang<sup>\*a</sup>

Nanoscale sorption is a promising strategy for catalyst and purification system design. In this paper, cellulose nanofibrils (CNFs) were densely attached with aldehyde functional groups on the surface via a mild periodate oxidation process, and then applied as mesoporous sorbents to remove Cu(II) and Pb(II) from aqueous solutions. In the studied concentration range (0.6–1.0 mmol L<sup>-1</sup>), a removal capacity of 0.75 mmol g<sup>-1</sup> for Pb(II) and 0.58 mmol g<sup>-1</sup> for Cu(II) was obtained. It is higher than most reported results over a much broader concentration range. Furthermore, the physical chemistry of the sorption process was studied in terms of sorption kinetics, sorption isotherm study and thermodynamic study. The results showed that the sorption process is under the combined influences of reaction kinetics, film diffusion and intraparticle diffusion, and follows the Langmuir model of monolayer adsorption. The sorption is spontaneous and endothermic. This development demonstrates an ecofriendly and cost-effective method with high level effectiveness of metal ion removal.

Received 15th August 2016  
Accepted 21st September 2016

DOI: 10.1039/c6ra20598d

[www.rsc.org/advances](http://www.rsc.org/advances)

## 1. Introduction

Heavy metal ions are common pollutants in the aquatic environment. The accumulation of excessive heavy metals, such as Pb(II), Cu(II), Cd(II), Hg(II) and Ni(II), in human bodies can cause deleterious health issues.<sup>1</sup> Removal of heavy metal ions from water is an essential environmental issue. Generally, metal ions can be removed from water through chemical precipitation, ion exchange, membrane filtration, adsorption, *etc.*<sup>2,3</sup> Cellulose, the most earth-abundant, renewable, eco-friendly polymer, has been extensively studied for heavy metal removal. Cellulose consists of linear chains of repeating β-D-glucopyranose units covalently linked through 1,4-glycosidic bonds. Each β-D-glucopyranose repeating unit possesses hydroxyl groups at the C-2, C-3, and C-6 positions, and one end of the chain has a free hemiacetal (or aldehyde) group at C-1, which is thus called the reducing end.<sup>4</sup> The hydroxyl groups on cellulose are of critical importance, as new functionalities can be introduced by reacting with these hydroxyls, thus generating a variety of products capable of chelating, electrostatically attracting, and ion-exchanging with heavy metals. Cellulose in the form of wood pulp or microcrystalline cellulose, or combined with other substances in cellulose-containing natural materials such as wood, husk, fruit peel, and sugar cane bagasse are usually modified or grafted with amino, carboxyl, isothiuronium,

mercapto, acrylic acid, acrylamide, or acrylonitrile groups for removal of heavy metal ions. The ionic species reported removable by cellulose include Cd(II), Cu(II), Ni(II), Pb(II), Zn(II), Cr(III), Cr(VI), and Hg(II), and the maximum removal capacity ranged from 0.01 mmol g<sup>-1</sup> to 8 mmol g<sup>-1</sup>.<sup>5,6</sup> Most of the reported cellulose sources for metal ions removal were conventional cellulose with dimensions in the micrometer scale. They are insoluble to most common inorganic/organic solvents and thus are difficult to form homogeneous dispersion solution, which imposes challenges to subsequent chemical functionalization, material structure fabrication, and further metal removal treatment. Additionally, their relatively large dimensions give rise to limited surface area and thus the low number of active sites for metal ion capture.

Recently, researchers disintegrated nanoscale cellulose from cellulose-containing materials and obtained cellulose nanofibrils (CNFs) and cellulose nanocrystals (CNCs).<sup>7–10</sup> These high-purity nanocelluloses are readily to form homogeneous colloidal dispersions in water as hydrogel due to their surface charges and nanoscopic dimensions. Nanocellulose is characterized by easy processing and high surface area, and thus can be advantageous in metal ions removal. Several pioneer works have successfully demonstrated the application of functionalized CNFs for removal of many different metal ions including Ag(I), Cd(II), Cu(II), Zn(II), Co(II), and Ni(II), Pb(II), Cr(III) and Au(III).<sup>11–17</sup> At low metal ions concentrations (≤1.01 mmol L<sup>-1</sup>), the metal ion sorption efficiencies were in the range of 27–100%. However, in order to reach high sorption efficiency, complex and multi-step chemical treatments were typically employed to functionalize CNF surfaces. It will be desirable,

<sup>a</sup>Department of Materials Science and Engineering, University of Wisconsin – Madison, Madison, WI 53705-2275, USA. E-mail: [xudong.wang@wisc.edu](mailto:xudong.wang@wisc.edu)

<sup>b</sup>Forest Products Laboratory, USDA Forest Service, Madison WI53726, USA. E-mail: [zcaif@fs.fed.us](mailto:zcaif@fs.fed.us)

however, for the functionalization process to be simple and cost-effective while still maintaining high level effectiveness of metal ion removal. In the area of cellulose chemistry, selective oxidation of cellulose by periodate is a simple and effective oxidation process. This reaction proceeds under mild aqueous conditions, and is characterized by selective cleavage of the cellulose C2 and C3 bonds with vicinal hydroxyl groups, without simultaneous occurrence of side reactions to any extent.<sup>18–21</sup> The resulting product has 2,3-dialdehyde units along the polymer chain. Aldehydes are very active reducing groups with a standard oxidation potential of +0.58 V, which are able to reduce metal ions including Hg(I), Pb(II), Cd(II), Ni(II), Cu(II), Pt(II), Ag(I), and Au(III) to their zero-valent forms.<sup>22,23</sup> In this work, we successfully implemented this simple one-step periodate oxidation process to introduce aldehyde groups onto CNFs. The dialdehyde CNFs (termed as DACs) were found very effective in removing two common heavy metal pollutants, Pb(II) and Cu(II), from water. Under the same metal ion concentration range (0.6–1.0 mmol L<sup>-1</sup>), we achieved a removal capacity of 0.75 mmol g<sup>-1</sup> for Pb(II) and 0.58 mmol g<sup>-1</sup> for Cu(II) that was higher than most reported results.<sup>11–16,21,24,25</sup> Compared to existing fabrication techniques, our approach is very effective for introducing functional groups to the surface of CNFs. Taking the advantage of the ultrasmall size of CNFs, the functional groups can reach an extremely high volume density, which would significantly enhance the functionality. Therefore, this cellulose processing technique is simple, cost-effective, and possesses high level effectiveness of metal ion removal, and holds great promises in ecofriendly nanomanufacture.

## 2. Experimental

### 2.1 Fabrication of aldehyde-functionalized nanocellulose sorbent

CNFs were prepared from wood pulp by tetramethylpiperidine-1-oxy (TEMPO)-mediated oxidation and subsequent mechanical homogenization following the method from Saito *et al.*<sup>8</sup> Commercially supplied, bleached, kraft eucalyptus pulps were oxidized in a mixture of TEMPO, sodium hypochlorite (NaClO), and sodium chlorite (NaClO<sub>2</sub>) under pH 6.8. The weight ratio was cellulose (dry weight of pulp) : TEMPO : NaClO : NaClO<sub>2</sub> = 1 : 0.016 : 0.07 : 1.13, and 0.05 M sodium phosphate buffer was added to form the final solution with the NaClO concentration being 0.1 M. The oxidation was carried out at 60 °C for 48 h. Oxidized pulps were then washed in distilled water and refined in a disk refiner. The refined fibers were subsequently subjected to centrifuge treatment to remove the supernatant fraction, and concentrated to 1 wt% using ultrafiltration. Finally, this suspension underwent high pressure mechanical homogenization by three pass-through of 200 and 87 μm microfluidizer chambers, mounted in series (M-110EH-30 Microfluidizer, Microfluidics, Newton, MA, USA). The resulting mixture of nanofibrils and water formed a transparent, stable aqueous colloid system (with a cellulose solid weight of 0.61%), termed as CNFs hydrogel. The CNFs hydrogel was stored at 4 °C for subsequent use. Carboxylate content of the as-processed CNFs hydrogel was determined to be ~0.65 mmol g<sup>-1</sup> using the

electric conductivity titration method.<sup>26</sup> Degree of polymerization (DP) of the CNFs hydrogel was estimated to be ~600, based on the intrinsic viscosity method.<sup>27</sup>

Sodium periodate (NaIO<sub>4</sub>) oxidation was performed on the isolated CNFs hydrogel to introduce aldehyde functionalities. Specifically, solid NaIO<sub>4</sub> was dissolved in water to form a 0.05 mol L<sup>-1</sup> solution. CNF hydrogels were immersed in the NaIO<sub>4</sub> solution for 20–300 hours in darkness, at room temperature. For each immersion, 20–30 g CNFs hydrogel was added into 18–27 mL NaIO<sub>4</sub> solution, and the dose ratio of NaIO<sub>4</sub> solution to CNFs hydrogel was fixed at 1.5 mole NaIO<sub>4</sub> per mole of cellulose glucopyranose unit. After the designed duration of oxidation, the hydrogels were taken out of solution and repeatedly rinsed to attain a neutral pH. Thereafter, the DACs hydrogels (as well as the pristine CNFs control sample) were freeze-dried to obtain porous DACs aerogels. Freezing was completed in several minutes by plunging the hydrogels into liquid nitrogen, and the frozen samples were then dried in a freeze-dryer (4.5 Liter FreeZone Freeze Dry System, Labconco, Kansas City, MO, US) of 35 mTorr chamber pressure, 15 °C chamber temperature, and –104 °C collector temperature. Under these conditions, ice within the samples directly sublimated and was then purged from the system.

### 2.2 Characterization

The amount of aldehyde groups on porous DACs and CNFs aerogels were determined by the Cannizzaro method. Cannizzaro reaction is a base-induced disproportionation of an aldehyde to an equal molar mixture of primary alcohol and carboxylic salt.<sup>28</sup> In the case of periodate-oxidized cellulose, the Cannizzaro reaction occurs with stoichiometric consumption of a mole of alkali per mole of dialdehyde unit.<sup>29,30</sup> Experimentally, a DACs aerogel was weighed, and treated with 0.05 M NaOH (volume denoted  $v_1$ , 5 mL). The stirred suspension was heated to 70 °C for 10 min, and then cooled to room temperature for 1–2 min. Subsequently, standardized 0.05 M HCl (volume denoted  $v_2$ , 6 mL) was added to the suspension, and excess of acid was titrated with standardized 0.01 M NaOH (volume denoted  $v_3$ ), using potassium hydrogen phthalate indicator to define the titration end-point. Aldehyde content present in the DACs aerogel was indicated by degree of oxidation (DO). DO, as the percentage of 2,3-dialdehyde units in glucopyranose repeat units of DACs was calculated according to

$$\text{DO} = \frac{0.01v_3 + 0.01v_1 - 0.05v_2}{m/198} \quad (1)$$

where  $m$  is the dry weight of porous DACs, and 198 is the average molecular weight of repeating unit in DACs. Three aliquots of sample were analyzed and we took the average for each reported DO value. Tollen's reagent was used to visualize the presence and distribution of aldehyde groups on DACs. The Tollen's reagent was prepared by adding 20% v/v aqueous ammonia to 1 wt% AgNO<sub>3</sub> water solution drop by drop to form clear solution, and it was freshly prepared for each use.

Morphology and elemental composition of the cellulose aerogels were characterized by LEO 1530 Gemini field emission

scanning electron microscope (SEM) coupled with energy dispersive spectroscopy (EDS). The crystallinity characteristics of the CNFs and DACs aerogels were analyzed using a Bruker D8 Discover X-ray diffractometer with  $\text{CuK}\alpha$  radiation ( $\lambda = 0.154$  nm) generated at 50 kV and 1 mA. The specific surface areas of the CNFs and DAC aerogels were measured using the Brunauer–Emmett–Teller (BET) method on a Quantachrome Autosorb-1 nitrogen gas sorption analyzer.

### 2.3 Sorption studies

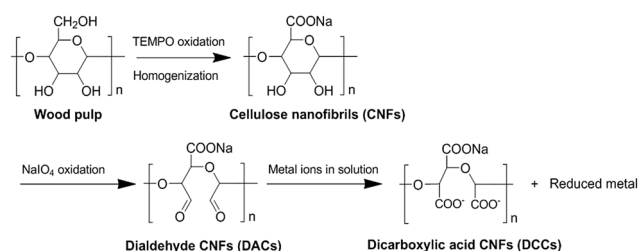
Stock solutions of  $\text{Cu}^{2+}$  and  $\text{Pb}^{2+}$  were prepared by dissolving copper acetate and lead nitrate in deionized (DI) water, respectively. Sodium acetate ( $0.174 \text{ mol L}^{-1}$ ) and acetic acid ( $0.100 \text{ mol L}^{-1}$ ) were used to adjust the pH value to  $4.6 \pm 0.1$ . Sorption was implemented by soaking DAC aerogel in 50 mL  $\text{Cu}^{2+}$  or  $\text{Pb}^{2+}$  stock solution under constant agitation at 180 rpm. The weight of DAC aerogel used in each sorption was controlled in the range of 25–40 mg. The effects of sorbent–solution contact time were studied at  $25^\circ\text{C}$ . The initial concentration of ion solutions was  $1.0 \text{ mmol L}^{-1}$  and initial pH value was 4.6. Contact time was set for 5 min, 15 min, 30 min, 45 min, 60 min, 75 min, 90 min, 120 min, 150 min, 180 min, 210 min, 240 min, 270 min, 300 min, 360 min, 420 min, 480 min, 540 min, and 600 min for each experiment. The influence of ion concentration was also investigated at  $25^\circ\text{C}$ . Initial ion concentration was set to  $0.3 \text{ mmol L}^{-1}$ ,  $0.4 \text{ mmol L}^{-1}$ ,  $0.5 \text{ mmol L}^{-1}$ ,  $0.6 \text{ mmol L}^{-1}$ ,  $0.7 \text{ mmol L}^{-1}$ ,  $0.8 \text{ mmol L}^{-1}$ ,  $0.9 \text{ mmol L}^{-1}$ ,  $1.0 \text{ mmol L}^{-1}$ ,  $2.0 \text{ mmol L}^{-1}$ ,  $3.0 \text{ mmol L}^{-1}$ ,  $4.0 \text{ mmol L}^{-1}$ ,  $5.0 \text{ mmol L}^{-1}$ , and  $6.0 \text{ mmol L}^{-1}$ . Initial pH of these solutions was in the range of 4.5 to 4.7 and remained in this range after sorption. Contact time was fixed at 360 min, because this contact time proved to be long enough to reach sorption equilibrium for all solutions. Effects of temperature on sorption process were investigated under  $25^\circ\text{C}$ ,  $35^\circ\text{C}$ ,  $45^\circ\text{C}$ , and  $55^\circ\text{C}$ . Ion solutions with initial concentration of  $1.0 \text{ mmol L}^{-1}$  and initial pH value of 4.6 were used under a fixed contact time of 360 min.

Two identical sorption experiments were performed for each condition. The resultant solutions were filtered through nylon syringe filters (pore size of  $0.45 \mu\text{m}$ ). Blank experiments showed that the nylon filters adsorbed neither  $\text{Cu}(\text{II})$  nor  $\text{Pb}(\text{II})$ . Solutions were diluted to  $0.5\text{--}2 \text{ mg L}^{-1}$  in 4%  $\text{HNO}_3$  for determination of residual metal concentration by inductively coupled plasma optical emission spectrometry (Vista-MPX ICP-OES, Varian Inc., Palo Alto, USA). Cu was analyzed at a wavelength of 324.754 nm, and Pb was analyzed at 220.353 nm. Concentrations were analyzed based on intensity of the spectra at these wavelengths. Spectral interference of the sodium element, which possibly exists in our sample solutions, was insignificant at the chosen wavelengths. Standard solutions covering the probable concentration range of Cu and Pb in solutions were prepared by diluting commercial 1000 ppm standards with 4%  $\text{HNO}_3$  to make a working curve. Standard solutions and the  $\text{HNO}_3$  blank were re-analyzed after running every 40 samples to check for instrument drift. Three aliquots were analyzed for each sample solution. Relative standard deviation (RSD) was less than 3% for all the analyses.

## 3. Results and discussions

DACs were fabricated by oxidizing CNFs with sodium periodate and the corresponding reaction procedure is shown in Scheme 1. In this process, sodium periodate selectively oxidized the secondary hydroxyls and thus cleaved the C2–C3 bonding, yielding a product with 2,3-dialdehyde units along the polymer chain. The periodate oxidation process was studied by analyzing DO of DACs as a function of time under fixed periodate oxidant concentration and reactants molar ratio. As shown in Fig. 1a, DO increased gradually with oxidation time. After 100 h oxidation, more than 50% of the glucopyranose repeating units were converted to noncyclic 2,3-dialdehyde structures. 180 h oxidation treatment resulted in a DO value of 81.6%. The DO value appeared approaching a saturation point of  $\sim 84\%$  with extended oxidation time. Due to the mild oxidation conditions, DACs remained as integral hydrogels after the treatments. However, the hydrogels shrunk to  $\sim 90\%$  of its original volume after 180 h oxidation, and only  $\sim 50\%$  after 220 h oxidation. The shrinkage could result from buckling of the open-ring 2,3-dialdehyde structures,<sup>31,32</sup> as well as reduced hydrophilicity of the hydrogel and thus its ability of holding water when hydroxyl groups were converted to aldehyde groups. XRD analysis was performed to study the effects of periodate oxidation on crystalline structure of the cellulose. As shown in Fig. 1b, the CNFs aerogel showed a XRD pattern with a wide peak at  $2\theta = 22.7^\circ$ , which was attributed to the diffraction from (200) from semi-crystalline cellulose  $\text{I}\beta$ .<sup>33,34</sup> The crystalline part was formed due to the inter- and intra-cellulose chain hydrogen bonding occurring among the hydroxyl groups. It was observed that the peak intensity of DACs obtained from different oxidation period was decreased compared to CNFs, and the longer the oxidation period, the weaker the peak was. It is due to the fact that the oxidation treatment opened the pyranose ring and consumed the hydroxyl groups. The crystalline structure was thus destroyed to some extent, giving rise to larger portion of amorphous phase in the material. For DACs obtained from 140 h and 180 h oxidation, the peak at  $2\theta = 22.7^\circ$  was still sharp, indicating a large amount of crystalline structure of cellulose was well preserved. Due to the fact that 180 h periodate oxidation treatment gave rise to DACs with a high DO and well-preserved hydrogel morphology and crystalline structure, the 180 h DACs samples were used in all of the metal sorption studies.

Nitrogen gas BET surface area measurements were conducted to determine the surface areas of the aerogels. Nitrogen



Scheme 1 Fabrication of DACs from CNFs, and applications of the former to metal ions sorption.

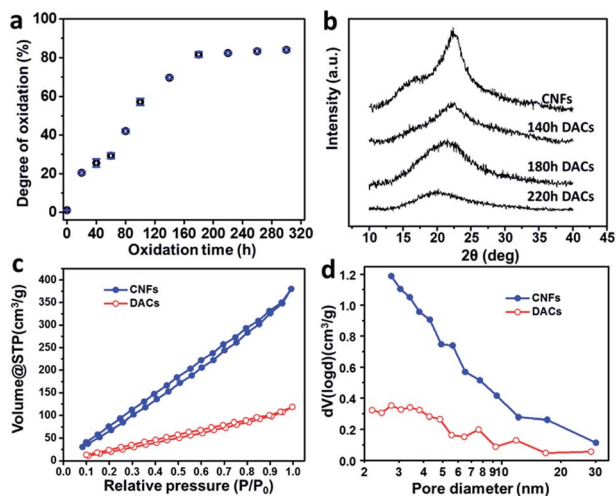


Fig. 1 (a) Degree of periodate oxidation of CNFs as a function of the oxidation time. (b) XRD pattern of CNFs, and DACs synthesized from different oxidation time. (c) Nitrogen adsorption-desorption isotherms measured from 180 h DACs and CNFs samples. (d) Corresponding pore size distributions of DACs and CNFs samples.

adsorption-desorption isotherms and pore size distributions were shown in Fig. 1c and d, and the specific area for CNFs and DACs aerogels was  $185.1 \text{ m}^2 \text{ g}^{-1}$  and  $134.4 \text{ m}^2 \text{ g}^{-1}$ , respectively. Both of these surface area values are high, and the reduction in surface area after the oxidation treatment is possibly due to the buckling effects and the decreased hydrophilicity of dialdehyde groups as mentioned earlier.

SEM confirmed that 180 h oxidation treatment exerted insignificant influence on the cellulose porous structure. A typical CNFs aerogel presented sheet-like aggregated morphology (inset of Fig. 2a). Zoom-in SEM image showed

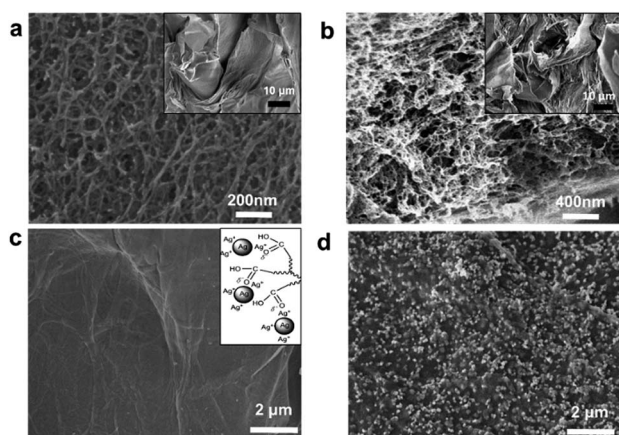


Fig. 2 SEM images of as-prepared CNFs (a) and DACs (b) showing the mesoporous network structure before and after oxidation. Insets in (a) and (b) are low-magnification SEM images showing the laminated microstructure. (c) CNFs surface after Tollen's reagent treatment showing sparsely deposited Ag nanoparticles. Inset schematically shows the interaction between  $\text{Ag}^+$  ions and aldehyde groups. (d) DACs after Tollen's reagent treatment showing a large amount of Au nanoparticle that were uniformly distributed on the surface.

aggregates were composed of interconnecting fibrous networks (Fig. 2a). Microstructure after oxidation is shown in Fig. 2b. The same sheet-like aggregates (inset of Fig. 2b) and mesoscale fiber network can be clearly observed. This evidenced the periodate oxidation process did not impose significant morphology change to the cellulose microstructure.

Tollen's reagent was then employed to visualize the presence and distribution of aldehyde groups on DACs, because the diamminesilver  $[\text{Ag}(\text{NH}_3)_2]^+$  in the reagent can easily oxidize aldehyde groups and form zero-valence Ag (inset of Fig. 2c). In our study, both CNFs and DACs hydrogels were immersed into Tollen's reagent separately. After 1 hour immersion, transparent CNFs hydrogel showed no obvious coloration while transparent DACs hydrogel turned black. SEM imaging showed only a few particles were generated on CNFs surfaces (Fig. 2c), while a large number of nanoparticles were observed on DACs. These nanoparticles were uniformly distributed on the surface of and within the DACs sheets (Fig. 2d). This comparison revealed DACs hydrogel carried a large amount of aldehyde groups from the periodate oxidation.

Porous DACs aerogels were then used to remove  $\text{Cu}(\text{II})$  and  $\text{Pb}(\text{II})$  from aqueous solutions. As shown in Fig. 3a, sorption amount increased rapidly in the beginning when DACs sorbents were immersed in  $\text{Cu}(\text{II})$  and  $\text{Pb}(\text{II})$  solutions, and then gradually reached an equilibrium value. The initial large sorption rate was attributed to large amounts of available functionality sites when first placed in solution. Both  $\text{Cu}(\text{II})$  and  $\text{Pb}(\text{II})$  sorption systems reached equilibrium after 5 h, where  $\sim 58.60\%$   $\text{Cu}(\text{II})$  and  $\sim 75.09\%$   $\text{Pb}(\text{II})$  were removed from the solution. Given the amount of CNF material being used, the removal capacity was found to be  $0.75 \text{ mmol g}^{-1}$  for  $\text{Pb}(\text{II})$  and  $0.58 \text{ mmol g}^{-1}$  for  $\text{Cu}(\text{II})$ . Compared to previous reports, our porous DACs aerogels was fabricated through a simple step of oxidation under mild conditions and yielded generally higher removal efficiency. Examples includes advanced nanocellulose-derived sorbents

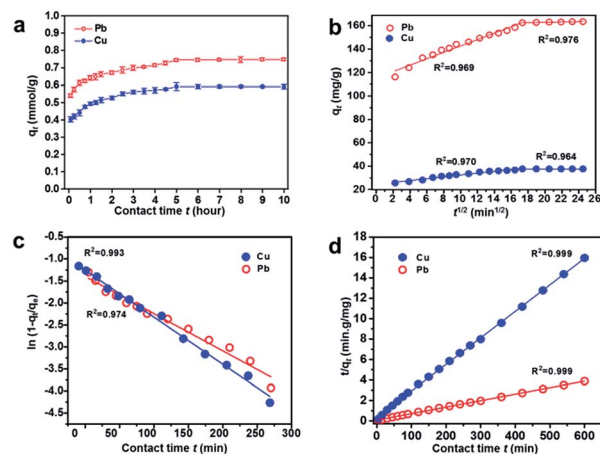


Fig. 3 (a) The sorption amount as a function of sorbent-solution contact time. (b) Numerical fitting of the sorption data to the intra-particle diffusion model showing two sloped segments. (c) Fitting to the film diffusion model for the first 5 hours of sorption; (d) fitting to the pseudo-2nd-order model for the entire sorption period.

with functional groups of sulfite ions<sup>16</sup> (0.54 mmol g<sup>-1</sup> Au(III)), carboxyl groups<sup>12</sup> (0.004 mmol g<sup>-1</sup> Cu(II)), or poly(acrylic acid) and poly(acrylic acid)/sodium humate<sup>35</sup> (0.12 mmol g<sup>-1</sup> Cu(II)), as well as more complexly treated cellulose by multi-step reactions (e.g. 0.41 mmol g<sup>-1</sup> Pb(II) and 1.02 mmol g<sup>-1</sup> Cu(II);<sup>24</sup> 1.3 mmol g<sup>-1</sup> Hg(II);<sup>21</sup> 0.06 mmol g<sup>-1</sup> Pb(II) and 0.25 mmol g<sup>-1</sup> Cu(II)<sup>25</sup>).

Numerical analyses were performed to gain insights into physical chemistry of the sorption process and to reveal if they were controlled by reaction kinetics, and/or film diffusion, and/or intraparticle diffusion. The Weber and Morris method<sup>36–39</sup> was first used to analyze the diffusion process. According to this method, the sorption amount  $q_t$  (mg g<sup>-1</sup>) of both Cu(II) and Pb(II) is plotted against the square root of time  $t^{0.5}$  (min<sup>0.5</sup>), as shown in Fig. 3b. A linear relation was obtained from both metals, and linear fitting curves did not pass the origin, indicating there was a certain degree of film diffusion control, in addition to intraparticle diffusion in both cases. Additionally, both curves showed two linear regions where the initial segment had a relatively large slope but the latter segment was nearly flat. The presence of two slopes suggests two steps were involved in the sorption process. The sloped segment could correspond to a film diffusion dominated case; while the flat segment represents the intraparticle diffusion controlled process.

To further confirm the sorption mechanism of the initial sloped region, the first 5 h data were fitted to the film diffusion rate model,<sup>37,40</sup> where  $\ln(1 - q_t/q_e)$  was plotted against time  $t$  ( $q_e$  and  $q_t$  are the amount of ions sorbed at equilibrium and at time  $t$ , respectively). Fractional attainment of the equilibrium ( $q_t/q_e$ ) term is related to the concentration gradient in liquid film surrounding the sorbent, which is more specific to film diffusion controlled processes. As shown in Fig. 3c, the fitting gave high correlation coefficients ( $R^2 > 0.97$ ) for both Cu(II) and Pb(II), suggesting that the initial sorption was controlled by film diffusion. It should be pointed out that pseudo-first order model can also fit the data for first-hours sorption. However, it is more of an empirical equation, and not able to provide very insightful mechanisms for the sorption process. Therefore, our discussion here only focuses on the diffusion model.

From above, it is reasonable to conclude, the sorption of Cu(II) and Pb(II) on DACs sorbents are initially controlled by film diffusion and later by intraparticle diffusion. In the first few hours, metal ions may only occupy the aldehyde sites near the external surface of the sorbent. In this process, transfer of metal ions within the pores could be very fast, hence, the sorption rate was determined by diffusion across boundary layers of the fluids surrounding external surfaces of the sorbent, *i.e.* film diffusion. As the sorption proceeded, all available surface sites became occupied and metal ions penetrated deeply within the sorbent through mesoscopic channels. This process could be much slower and the intraparticle diffusion now became the rate-limiting mechanism.

Upon sorption, the removal of metal ions by DACs was mainly attributed to chemical interactions between the aldehyde functional groups and metal ions. In this regard, pseudo-second-order model<sup>37,41–43</sup> was used to describe the metal ion removal processes. A pseudo-second-order model has the linear form of

$$\frac{t}{q_t} = \frac{1}{k_2 q_e^2} + \frac{t}{q_e} \quad (2)$$

where  $q_e$  and  $q_t$  are the amount of ions sorbed at equilibrium and at time  $t$  (min), and  $k_2$  is the pseudo-second-order rate constant. As shown in Fig. 3d,  $t/q_t$  was plotted against time  $t$  for both Cu(II) and Pb(II) sorption cases. Both fitted lines demonstrated high correlation coefficients ( $>0.99$ ) indicating that the pseudo-second-order model is valid for describing the kinetic sorption processes and chemical interactions involved in the sorption processes. The theoretical maximum sorption capacity  $q_e$  revealed by data fitting was 38.46 and 157.73 mg g<sup>-1</sup> for Cu(II) and Pb(II), respectively. These values matched well to the equilibrium sorption capacities obtained experimentally (37.21 and 155.58 mg g<sup>-1</sup> for Cu(II) and Pb(II), respectively).

The effects of ion concentration on sorption amounts were shown in Fig. 4a at different temperatures. Each of the sorption amounts was obtained under equilibrium condition. The equilibrium was confirmed by the fact that the sorption amount showed no further increase after extended immersion hours in solutions. As the concentration increased from 0.3 to 6.0 mmol L<sup>-1</sup> at 25 °C, the sorption amount of Cu(II) and Pb(II) increased from 15.60 to 24.64 mg g<sup>-1</sup> and from 64.86 to 160.65 mg g<sup>-1</sup>, respectively (Fig. 4a and b). Monotonic increase of the sorption amount with solution concentration was a result of the high sorption capacity of mesoporous DACs sorbents.

The sorption isotherm was then analyzed using the Langmuir model<sup>44</sup> and Freundlich model<sup>45,46</sup> to understand how adsorbents were distributed between the solution and sorbent solids at equilibrium. The Langmuir isotherm is based on monolayer adsorption occurring at energetically equivalent sites of the sorbent (*i.e.*, constant heat of adsorption for all sites). It has a mathematical form of

$$\frac{C_e}{q_e} = \frac{C_e}{q_{\max}} + \frac{1}{k_L q_{\max}} \quad (3)$$

where  $C_e$  is the concentration at equilibrium,  $q_{\max}$  is the maximum capacity that the system can reach, and  $k_L$  is the Langmuir constant. Freundlich isotherm assumes that the

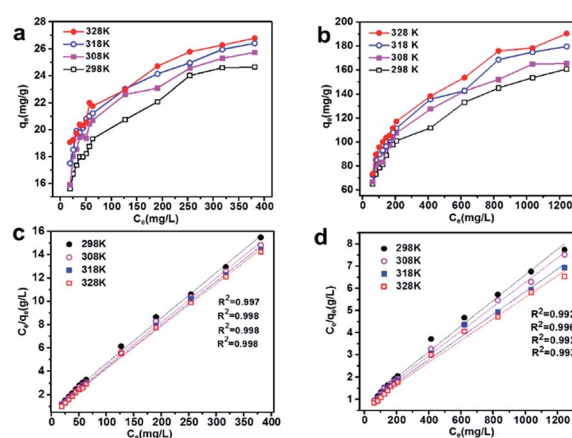


Fig. 4 Sorption isotherm of Cu (a) and Pb (b) at different temperatures, and Langmuir fitting of the isotherm data of Cu (c) and Pb (d).

Table 1 Thermodynamic parameters of Cu(II) and Pb(II) sorption on DACs at different temperatures

Heavy metal	T (K)	$k_L$	Langmuir $q_{max}$	$k_d$	$\ln k_d$	$\Delta G^\circ$ (kJ mol <sup>-1</sup> )	$\Delta H^\circ$ (kJ mol <sup>-1</sup> )	$\Delta S^\circ$ (kJ mol <sup>-1</sup> )
Cu(II)	298	0.05315	25.6	4.09	1.41	-3.49	9.80	0.045
	308	0.06176	26.4	4.61	1.53	-3.92		
	318	0.06639	27.0	5.41	1.69	-4.47		
	328	0.06792	27.4	5.79	1.76	-4.79		
Pb(II)	298	0.00713	172.7	1.47	0.39	-0.95	2.23	0.011
	308	0.00739	181.2	1.51	0.41	-1.06		
	318	0.00701	195.3	1.54	0.43	-1.14		
	328	0.00701	204.5	1.60	0.47	-1.28		

active sites on the sorbent are heterogeneous, and the sorption process is reversible and multilayer. It follows the relation of:

$$\lg q_e = \lg k_F + \frac{1}{n} \lg C_e \quad (4)$$

where  $k_F$  is Freundlich constant, and  $n$  is the heterogeneity constant. Our experimental data were plotted based on both Langmuir and Freundlich models. The Freundlich fittings ( $\lg q_e$  versus  $\lg C_e$ ) were nonlinear and gave very low correlation coefficients (less than 0.5). On the other hand, the fittings with Langmuir model ( $C_e/q_e$  versus  $C_e$ ) at all temperatures were of high correlation coefficients for both Cu(II) and Pb(II) (Fig. 4c and d, and values for Langmuir parameter  $k_L$  and  $q_{max}$  were listed in Table 1), suggesting the sorption process was monolayer and all sorption sites (*i.e.* the aldehyde functional groups) were equivalent, and the distribution of aldehydes was homogeneous and uniform. Uniform distribution of aldehydes could be attributed to the complete conversion of secondary hydroxyl groups that are evenly distributed on each anhydroglucopyranose unit of cellulose molecules. Homogeneity and uniformity of aldehydes were also supported by the uniform coverage and narrow size distribution of Ag nanoparticles that were produced by DACs aerogel reduction (Fig. 2d).

Fig. 4 also revealed that at the four testing temperatures, isotherms showed the same trend for both Cu(II) and Pb(II) sorption, suggesting that the sorption mechanism of DACs was independent of temperature within the study range. However, the sorption amount of both Cu(II) and Pb(II) increased slightly as temperature increased. This could be a result of enhanced metal ions mobility at higher temperature and endothermic nature of the sorption process. To better understand the temperature influences, thermodynamics parameters were calculated based on equilibrium data and the thermodynamic equilibrium constants.

According to Khan and Singh's method,<sup>47,48</sup> the thermodynamic equilibrium constant  $k_d$  can be obtained from the intercept of plots  $\ln(q_e/C_e)$  against  $q_e$  (Fig. 5a and b, value of  $k_d$  were listed in Table 1). By plotting  $\ln k_d$  versus  $1/T$  (Fig. 5c), enthalpy change  $\Delta H^\circ$ , and entropy change  $\Delta S^\circ$  in the sorption process can be determined according to following equation:

$$\ln k_d = -\frac{1}{RT} \Delta G^\circ = \frac{\Delta S^\circ}{R} - \left(\frac{\Delta H^\circ}{R}\right) \frac{1}{T} \quad (5)$$

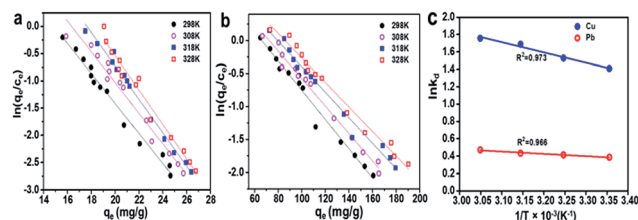


Fig. 5 Plots of  $\ln(q_e/C_e)$  versus  $q_e$  for Cu (a) and Pb (b); plots of  $\ln k_d$  versus  $1/T$  (c) for the determination of thermodynamic parameters.

Obtained values for all thermodynamics related parameters were listed in Table 1. The results showed that  $\Delta G^\circ$  was negative for all testing temperatures, and became increasingly negative when temperatures increased. This discovery suggests that the sorption processes of Cu(II) and Pb(II) on DACs were spontaneous.  $\Delta H^\circ$  for both Cu(II) and Pb(II) were found positive, indicative of the endothermic nature of sorption processes. This also supported the earlier finding that the equilibrium sorption amount increased with increasing temperature.  $\Delta S^\circ$  for both metal ions were positive, which agrees with a previously reported work<sup>49</sup> on the adsorption of Cu(II) by wood sawdust. According to that work, the positive change of entropy might be a result of redistribution of energy between the adsorbate and the adsorbent.

## 4. Conclusions

In summary, a mesoporous DACs aerogel was fabricated by periodate oxidation of CNFs hydrogel followed by freeze-drying. It exhibited BET specific area of 134.4 m<sup>2</sup> g<sup>-1</sup> and was able to effectively remove Cu(II) and Pb(II) ions from their corresponding aqueous solutions. Kinetic studies showed that the entire sorption process was of pseudo-second-order in terms of reaction kinetics and the theoretical maximum sorption capacity was 38.36 mg g<sup>-1</sup> and 157.73 mg g<sup>-1</sup> for Cu(II) and Pb(II), respectively. Numerical analyses revealed that the sorption was initially film-diffusion limited and later intraparticle-diffusion limited: the diffusion of metal ions across liquid films surrounding the DACs sorbents determined the sorption rate in the first 5 h, while diffusion of metal ions through the mesoscopic channels within the DACs limited the later sorption rate. Sorption equilibrium studies found that experimental data at equilibrium fitted well to the Langmuir isotherm model for

both metal ions, indicating the chemisorption process was monolayer and all aldehyde sorption sites were equivalent. Thermodynamic calculations under different temperatures all gave negative  $\Delta G^\circ$  and positive  $\Delta H^\circ$  values, suggesting the spontaneous and endothermic nature of the sorption process of both Cu(II) and Pb(II). Development of mesoporous DACs aerogel offers a simple and effective pathway to remove heavy metal ions from aqueous solutions.

## Acknowledgements

The authors thank the supported from the Forest Product Laboratory under Award # 14-JV-1111124-029 and National Science Foundation (NSF) under award # CMMI-1148919. Chunhua Yao appreciates the helpful discussions with Dr Shuguang Zhang in Department of Chemical Engineering at Shandong University of Technology (China).

## Notes and references

- R. Singh, N. Gautam, A. Mishra and R. Gupta, *Indian J. Pharmacol.*, 2011, **43**, 246–253.
- M. Bilal, J. A. Shah, T. Ashfaq, S. M. H. Gardazi, A. A. Tahir, A. Pervez, H. Haroon and Q. Mahmood, *J. Hazard. Mater.*, 2013, **263**, 322–333.
- M. Barakat, *Arabian J. Chem.*, 2011, **4**, 361–377.
- D. Klemm, *Comprehensive Cellulose Chemistry 1, Fundamentals and Analytical Methods*, 1998.
- M. A. Hubbe, S. H. Hasan and J. J. Ducoste, *BioResources*, 2011, **6**, 2161–2287.
- D. W. O'Connell, C. Birkinshaw and T. F. O'Dwyer, *Bioresour. Technol.*, 2008, **99**, 6709–6724.
- T. Saito, S. Kimura, Y. Nishiyama and A. Isogai, *Biomacromolecules*, 2007, **8**, 2485–2491.
- T. Saito, M. Hirota, N. Tamura, S. Kimura, H. Fukuzumi, L. Heux and A. Isogai, *Biomacromolecules*, 2009, **10**, 1992–1996.
- Y. Habibi, L. A. Lucia and O. J. Rojas, *Chem. Rev.*, 2010, **110**, 3479–3500.
- D. Klemm, F. Kramer, S. Moritz, T. Lindström, M. Ankerfors, D. Gray and A. Dorris, *Angew. Chem., Int. Ed.*, 2011, **50**, 5438–5466.
- P. Liu, H. Sehaqui, P. Tingaut, A. Wichser, K. Oksman and A. P. Mathew, *Cellulose*, 2014, **21**, 449–461.
- S. Hokkanen, E. Repo and M. Sillanpää, *Chem. Eng. J.*, 2013, **223**, 40–47.
- S. Hokkanen, E. Repo, T. Suopajarvi, H. Liimatainen, J. Niinimaa and M. Sillanpää, *Cellulose*, 2014, **21**, 1471–1487.
- S. Nagpal, A. Kardam, M. Gera and V. Jain, *Environ. Technol.*, 2015, **36**, 706–714.
- X. Zhang, J. Zhao, L. Cheng, C. Lu, Y. Wang, X. He and W. Zhang, *RSC Adv.*, 2014, **4**, 55195–55201.
- A. D. Dwivedi, S. P. Dubey, S. Hokkanen and M. Sillanpää, *Chem. Eng. J.*, 2014, **253**, 316–324.
- A. Sheikhi, S. Safari, H. Yang and T. G. van de Ven, *ACS Appl. Mater. Interfaces*, 2015, **7**, 11301–11308.
- E. Maekawa and T. Koshijima, *J. Appl. Polym. Sci.*, 1984, **29**, 2289–2297.
- A. Varma and M. Kulkarni, *Polym. Degrad. Stab.*, 2002, **77**, 25–27.
- J. A. Sirviö, A. Kolehmainen, M. Visanko, H. Liimatainen, J. Niinimäki and O. E. Hormi, *ACS Appl. Mater. Interfaces*, 2014, **6**, 14384–14390.
- S. Kumari and G. S. Chauhan, *ACS Appl. Mater. Interfaces*, 2014, **6**, 5908–5917.
- P. Vanysek, *CRC Handbook of Chemistry and Physics*, 1998.
- G. Karp, *Cell and Molecular Biology: Concepts and Experiments*, 2002.
- R. Saravanan and L. Ravikumar, *J. Water Resour. Prot.*, 2015, **7**, 530–545.
- C. Zang, D. Zhang, J. Xiong, H. Lin and Y. Chen, *J. Eng. Fiber. Fabr.*, 2014, **9**, 165–170.
- T. Saito and A. Isogai, *Biomacromolecules*, 2004, **5**, 1983–1989.
- W. Alexander, O. Goldschmid and R. Mitchell, *Ind. Eng. Chem.*, 1957, **49**, 1303–1306.
- T. Geissman, *Org. React.*, 1944, **2**, 94–113.
- B. Hofreiter, B. Alexander and I. Wolff, *Anal. Chem.*, 1955, **27**, 1930–1931.
- K. Pommerening, H. Rein, D. Bertram and R. Müller, *Carbohydr. Res.*, 1992, **233**, 219–223.
- P. RoyChowdhury and V. Kumar, *J. Biomed. Mater. Res., Part A*, 2006, **76**, 300–309.
- R. Guthrie, *Adv. Carbohydr. Chem.*, 1961, **16**, 105–158.
- M. Wada and T. Okano, *Cellulose*, 2001, **8**, 183–188.
- Y. Nishiyama, P. Langan and H. Chanzy, *J. Am. Chem. Soc.*, 2002, **124**, 9074–9082.
- X. Zhang, J. Zhao, L. Cheng, C. Lu, Y. Wang, X. He and W. Zhang, *RSC Adv.*, 2014, **4**, 55195–55201.
- W. J. Weber and J. C. Morris, *J. Sanit. Eng. Div., Am. Soc. Civ. Eng.*, 1963, **89**, 31–60.
- Y. Ho, J. Ng and G. McKay, *Sep. Purif. Rev.*, 2000, **29**, 189–232.
- V. Poots, G. McKay and J. Healy, *Water Res.*, 1976, **10**, 1061–1066.
- E. Rubín, P. Rodríguez, R. Herrero and M. E. Sastre de Vicente, *J. Chem. Eng. Data*, 2010, **55**, 5707–5714.
- G. Boyd, A. Adamson and L. Myers Jr, *J. Am. Chem. Soc.*, 1947, **69**, 2836–2848.
- Y. Ho and G. McKay, *Water Res.*, 1999, **33**, 578–584.
- Y.-S. Ho and G. McKay, *Process Biochem.*, 1999, **34**, 451–465.
- G. Blanchard, M. Maunaye and G. Martin, *Water Res.*, 1984, **18**, 1501–1507.
- I. Langmuir, *J. Am. Chem. Soc.*, 1916, **38**, 2221–2295.
- V. Poots, G. McKay and J. Healy, *J. - Water Pollut. Control Fed.*, 1978, **50**, 926–935.
- S. J. Allen, G. McKay and K. Khader, *J. Chem. Technol. Biotechnol.*, 1989, **45**, 291–302.
- A. A. Khan and R. Singh, *Colloids Surf.*, 1987, **24**, 33–42.
- S. Lyubchik, A. Lyubchik, I. Fonseca, O. Lygina and S. Lyubchik, *Thermodynamics: Interaction Studies-Solids, Liquids, and Gases*, 2011.
- M. E. Argun, S. Dursun, C. Ozdemir and M. Karatas, *J. Hazard. Mater.*, 2007, **141**, 77–85.